OAK RIDGE NATIONAL LABORATORY LIBRARIES
3 4456 0555807 2

CENTRAL RESEARCH LIBRARY

ORNL/TM-5661

Cy 47

An Estimate of Thermoelastic Heat Production from Superconducting Composites in Pulsed Poloidal Coil Systems

J. K. Ballou W. H. Gray

OAK RIDGE NATIONAL LABORATORY
CENTRAL RESEARCH LIBRARY
DOCUMENT COLLECTION
LIBRARY LOAN COPY
DO NOT TRANSFER TO ANOTHER PERSON
If you wish someone else to see this document, send in name with document and the library will arrange a loan.

OAK RIDGE NATIONAL LABORATORY
OPERATED BY UNION CARBIDE CORPORATION FOR THE ENERGY RESEARCH AND DEVELOPMENT ADMINISTRATION

Printed in the United States of America. Available from
National Technical Information Service
U.S. Department of Commerce
5285 Port Royal Road, Springfield, Virginia 22161
Price: Printed Copy $3.50; Microfiche $2.25

This report was prepared as an account of work sponsored by the United States Government. Neither the United States nor the Energy Research and Development Administration/United States Nuclear Regulatory Commission, nor any of their employees, nor any of their contractors, subcontractors, or their employees, makes any warranty, express or implied, or assumes any legal liability or responsibility for the accuracy, completeness or usefulness of any information, apparatus, product or process disclosed, or represents that its use would not infringe privately owned rights.

ORNL/TM-5661

Contract No. W-7405-eng-26

AN ESTIMATE OF THERMOELASTIC HEAT PRODUCTION FROM SUPERCONDUCTING COMPOSITES IN PULSED POLOIDAL COIL SYSTEMS

J. K. Ballou and W. H. Gray
Magnetics & Superconductivity Section
Thermonuclear Division

Date Published: November 1976

Paper Presented at the 2nd ANS Topical Meeting on the Technology of Controlled Thermonuclear Fusion, Richland, Washington

NOTICE This document contains information of a preliminary nature and was prepared primarily for internal use at the Oak Ridge National Laboratory. It is subject to revision or correction and therefore does not represent a final report.

OAK RIDGE NATIONAL LABORATORY
Oak Ridge, Tennessee 37830
operated by
UNION CARBIDE CORPORATION
for the
ENERGY RESEARCH AND DEVELOPMENT ADMINISTRATION

OAK RIDGE NATIONAL LABORATORY LIBRARIES
3 4456 0555807 2

AN ESTIMATE OF THERMOELASTIC HEAT PRODUCTION FROM SUPERCONDUCTING COMPOSITES IN PULSED POLOIDAL COIL SYSTEMS*

J. K. Ballou and W. H. Gray

Oak Ridge National Laboratory
Oak Ridge, Tennessee 37830

In the design of the cryogenic system and superconducting magnets for the poloidal field system in a tokamak, it is important to have an accurate estimate of the heat produced in superconducting magnets as a result of rapidly changing magnetic fields. A computer code, PLASS[1] (Pulsed Losses in Axisymmetric Superconducting Solenoids), was written to estimate the contributions to the heat production from superconductor hysteresis losses, superconductor coupling losses, stabilizing material eddy current losses, and structural material eddy current losses.

Recently, it has been shown that thermoelastic dissipation in superconducting composites can contribute as much to heat production as the other loss mechanisms mentioned above.[2-4] We discuss a modification of PLASS which takes into consideration thermoelastic dissipation in superconducting composites. A comparison between superconductor thermoelastic dissipation and the other superconductor loss mechanisms is presented in terms of the poloidal coil system of the ORNL Experimental Power Reactor design.

I. INTRODUCTION

In the design of the cryogenic system and superconducting magnets for a poloidal field system in a tokamak, it is important to have an accurate estimate of the heat produced in the superconducting magnets as a result of the rapidly changing magnetic fields. Until recently, this estimate was obtained by assuming that the field was constant throughout the coil windings. A more accurate method of estimation involves integrating the losses over the coil windings, taking into account the spatial variation of the magnetic field. A computer code, PLASS (Pulsed Losses in Axisymmetric Superconducting Solenoids), was written to perform this integration.[1]

Recently, measurements[4] of stress-induced thermoelastic heat production in commercial superconducting composite wire indicated that this phenomenon could be a significant factor in the operation of large magnet systems where pulsed magnetic fields are encountered. For the poloidal coils of the ORNL Experimental Power Reactor (EPR),[5] the calculated stress-induced heating is the same order of magnitude as the other heat loads on the cryogenic system.

A computer program, PLSMOD, is described in this paper. PLSMOD is a modified version of PLASS which calculates pulsed

*Research sponsored by the Energy Research and Development Administration under contract with Union Carbide Corporation.

losses in superconducting solenoids due to thermoelastic dissipation, as well as three other types of superconducting magnet losses already calculated by PLASS. The basic loss mechanisms and calculational procedures programmed into PLASS are reviewed in Sects. II and III. The method used to calculate the thermoelastic heat production is described in Sect. IV and in Sect. V the heat generation from the various dissipative mechanisms is compared.

II. REVIEW OF THE LOSS MECHANISMS CODED INTO PLASS

The principal power loss mechanisms inherent in the design of the ORNL EPR poloidal coil system are superconductor hysteresis losses, superconductor coupling losses, stabilizing material eddy current losses, and structural material eddy current losses. The conductor specifications for this design are listed in Table 1. Figure 1 shows a schematic diagram of the conductor, which is composed of mixed-matrix Cu:CuNi:NbTi wires in a stainless steel conduit. The cable is cooled by forcing supercritical helium through the conduit and the interstices of the cable.[5,6]

The losses for this design are approximated using the following assumptions:

(a) For superconductors with small diameters, the hysteresis loss, W_H, per unit volume of superconductor for a cylical magnetic field variation from B_{min} to B_{max} and back to B_{min} can be expressed as[7,8]

$$\frac{W_H}{V} = \frac{\alpha_c}{2}\, d\, \ln\left(\frac{B_o + B_{max}}{B_o + B_{min}}\right) (\text{in J/m}^3) \quad , \qquad (1)$$

where V is volume, d is the superconductor filament diameter, and α_c and B_o are constants defined in the critical state equation

$$J_c(B) = \frac{\alpha_c}{B_o + B} \ (\text{in A/m}^2) \quad , \qquad (2)$$

where J_c is the critical current density for a magnetic field equal to B.

(b) The coupling losses are due to currents flowing through the matrix which have been induced by a perpendicular magnetic field. For a composite wire with radius r_o, the coupling energy loss, W_c, per unit volume is[9]

$$\frac{W_c}{V} = \frac{S}{V}\int_{t_i}^{t_{i+1}} \frac{\dot{B}^2}{2\rho_m}\, r_o^3 \left(\frac{1}{x_o^2} + \frac{1}{4}\right) dt \quad (\text{in J/m}^3) \quad , \qquad (3)$$

where S is the wire surface area, $\dot{B}$ is the derivative with respect to time of the perpendicular magnetic field, t is time, ρ_m is the matrix resistivity, x_o is the normalized twist pitch ($2\pi r_o/\ell_p$), and ℓ_p is the twist pitch length.

(c) The model for the structural material eddy current loss is a cylindrical conductor [as used in the ORNL Reference Design[5]] subjected to a time-varying magnetic field perpendicular to its axis. If the flux-penetration depth is assumed to be much longer than the cylinder size, the structural material eddy current loss, W_E, per unit volume can be conservatively estimated by

$$\frac{W_E}{V} = \int_{t_i}^{t_{i+1}} \frac{\dot{B}^2 R^2}{\rho_{ss}}\, dt \ (\text{in J/m}^3) \qquad (4)$$

where R is the radius of the cylinder and ρ_{ss} is the resistivity of the structural material.

III. NUMERICAL PROCEDURE

PLASS uses finite element techniques to numerically perform a two dimensional Gaussian axisymmetric integration on a body-of-revolution to obtain the individual values of the loss terms for a given time. If the current in a magnet is assumed to be linear function of time over a finite time increment, then the derivative of the current with respect to time and hence the derivative of the magnetic field with respect to time are constant in that time increment. Therefore, the differential times may be replaced with the difference between t_{i+1} and t_i. Further, we assume that the resistivities are not functions of magnetic field. These relationships are used to perform a piecewise linear integration in time to obtain the total energy loss for a particular poloidal field magnet system and pulse-time history.

The spatial variation of the magnetic field, which is taken into account directly during the Gaussian integration, is complicated by the fact that poloidal field magnet systems may have up to three distinct magnet sets [ohmic heating (OH), vertical field, and trim], each of which may have a different current versus time characteristic. The computer program linearly superimposes the magnetic field at a point due to each magnet set where each set may contain several poloidal magnets.

IV. THERMOELASTIC DISSAPATION CALCULATION PROCEDURE

The stress-induced heat production per unit volume is not obtained from an analytical model like those given for other losses in Sect. II, but is calculated by an empirical formula.[3] This formula, based on a cycle from 0.0 to maximum stress to 0.0, was coded into PLSMOD and has the forms

$$\frac{W_s}{V} = 50.0\ \sigma_{vm}^{1.183}\ ;\quad 0.0 < \sigma_{vm} < 200.0 \qquad (5)$$

and

$$\frac{W_s}{V} = 0.108\ \sigma_{vm}^{2.394}\ ;\ \sigma_{vm} > 200.0 \qquad (6)$$

where W_s is the stress induced heat production per unit volume, V, and σ_{vm} is the Von Mises stress. When using equations (5) and (6), the stress is expressed in units of megapascals and the resulting loss in units of joules per cubic meter.

In order to use the numerical procedure expressed in Sect. III to evaluate equations (5) and (6), a detailed finite element stress analysis must be performed. A previously developed finite element stress analysis computer code[10] was used to obtain the stress distribution throughout the magnet. It was decided not to merge the loss calculating code, PLSMOD, with the stress analysis code, MODEL, because of the individual program sizes.

Figure 2 is a flow chart of the major job steps necessary to execute these codes. As shown in Fig. 2, the only user-supplied data set is the original input data to PLSMOD. This fixed-format data set, PLASS.DAT, contains magnet geometrical and electrical information, superconductor constants, and mechanical property information.

The first execution of PLSMOD reads PLASS.DAT and then determines if the magnetic field has been calculated at each Gaussian integration point. If it has not, as would be the case for the first job step, three data sets are created. The first, PLASS.FLD, contains the magnetic field produced by each coil set at each Gaussian

integration point. The second, PLSMOD.FLD, contains the magnetic field at each Gaussian integration point for a particular time in a format acceptable to the finite element stress analysis code, MODEL. The third, MODEL.DAT, is an input data deck to the MODEL code.[11]

Execution of the second job step, MODPLS, runs the program MODEL with the previously created input data sets. MODEL creates two output data sets. The first, MODEL.OUT, is an output listing of the stress analysis. The second, MODEL.STR, contains the Von Mises stress at each Gaussian integration point.

Execution of the third job step, PLSMOD, runs program PLSMOD. PLSMOD reads the data sets PLASS.DAT, PLASS.FLD, and MODEL.STR. It then calculates the losses due to the four loss mechanisms discussed in this paper.

This procedure, we believe, is computationally efficient as the calculation of the magnetic field (by far the most time-consuming process) is performed only once. Further, changes in the mechanical or superconducting input properties may be made and results obtained without recalculation of the magnetic field.

V. CALCULATION OF THE ENERGY LOSS IN THE SUPERCONDUCTING POLOIDAL COIL SYSTEM OF THE ORNL EPR DESIGN

PLASS has been used to estimate the superconductor losses for the ohmic heating (OH) coil system for the latest ORNL EPR reference design.[6] The coil outlines of the OH system described in Ref. 6 are shown in Fig. 3. The area enclosed by the outline of each coil is proportional to the number of ampere-turns in that coil.

All of the magnets in the OH system are operated in the bipolar mode, i.e., the current in the coils is reversed during the duty cycle. The current waveform used in this study starts with full current in one direction and linearly changes to full current in the opposite direction in 2 sec. The current is increased slightly over the next 100 sec and is then returned to its initial state in 2 sec. The losses in the 100-sec period are negligibly small and are not calculated.

The total superconductor loss for this example is 2.26×10^5 J. In this design the helium present in the coil cannot be changed in one duty cycle and must absorb the total energy input. However, the refrigerator power is averaged over the longer period of time rather than over both of the 2-sec periods when the current is reversed. Over 100 sec, the average power is 2.26 kW.

The output of PLASS has been contoured to illustrate the distribution of energy input to the central solenoid due to superconductor losses. The contours of constant energy input (J/m^3) due to hysteresis losses are presented in Fig. 4. These losses are for the central solenoid only; the outboard coils are turned off. Near the midplane, the hysteresis losses are large at the inside radius of the windings and fall off rapidly towards the outside radius. Near the end of the solenoid the losses are large but do not decrease rapidly near the outside radius. As an example, consider two coil segments each 1/8 of the total solenoid length, one at the end and one at the midplane of the solenoid. The hysteresis losses in these segments are compared in Table 2. The hysteresis losses in the end segment are slightly larger than the losses in the middle segment. Figures 5 and 6

are contour plots of constant energy input for the coupling loss in the conductor and the eddy current losses in the stainless steel conduit, respectively. Figure 7 presents a contour plot of constant energy input per unit volume in the stress induced heat production. This contour is quite different from the preceding ones, since at a particular height the Von Mises stress distribution is relatively constant. The comparison of these losses in the middle and end segments is also given in Table 2.

A contour plot of the hysteresis losses in the central solenoid due to the other poloidal coils is given in Fig. 8. The hysteresis losses in the middle and end segments are about 15% of the hysteresis losses due to the self-field of the central solenoid (see Table 2). The total losses in the end segment are about 13% greater than the losses in the middle segment when all of the coils are considered.

For completeness, the contours of constant energy input for the coupling loss in the conductor, the eddy current loss in the stainless steel conduit, and the stress-induced heat production in the superconductor are presented in Figs. 9, 10, and 11, respectively.

VI. CONCLUSIONS

A computer code, PLASS, has been written to estimate the superconductor losses due to hysteresis, coupling, and stress-induced heating, as well as eddy current heating in the conductor design of the ORNL EPR. This code takes into account the spatial variation of the magnetic field in the coil windings and the time schedule for the current changes in up to three coil sets. PLASS has been used to estimate the heating due to superconductor losses in the ORNL EPR OH system and has shown that the losses in the central solenoid are nearly equally distributed through its windings.

NOMECLATURE

W = Energy

V = Volume (m^3)

B = Magnetic field

$\dot{B}$ = dB/dt (T/sec)

α_c = Constant defined in the critical-state equation (A T/m^2)

B_o = Constant defined in the critical-state equation (T)

$J_c(B)$ = Field dependent critical-current density (A/m^2)

P = Power (W)

S = Surface area (m^2)

r_o = Wire radius (m)

ρ_m = Matrix electrical resistivity (Ω-m)

x_o = $2\pi r_o/\ell_p$ = normalized twist length

ℓ_p = Twist pitch length (m)

ρ_{ss} = Structural electrical resistivity (Ω-m)

t = Time (sec)

σ = stress

REFERENCES

1. W. H. Gray and J. K. Ballou, paper presented at the 1976 Applied Superconductivity Conference, Stanford, CA, August 17–20, 1976 (proceedings to be published).
2. D. S. Easton, D. M. Kroeger, and A. Moazed, "Thermomechanical Heat Generation in Copper and a NbTi Superconducting Composite, Appl. Phys. Lett. 29(6) (1976).
3. J. E. Akin and A. Moazed, Thermoelastic Dissipation in Superconducting Materials, University of Tennessee, Knoxville, TN (February 1976).

4. D. M. Kroeger, D. S. Easton, and A. Moazed, "Stress-Induced Heating in Commercial Conductors and Its Possible Influence on Magnet Performance," paper presented at the 1976 Applied Superconductivity Conference, Stanford, CA, August 17–20, 1976 (proceedings to be published).
5. M. Roberts and E. S. Bettis (eds.), Oak Ridge Tokamak Experimental Power Reactor Study Reference Design, ORNL/TM-5042, Oak Ridge, TN (November 1975).
6. J. W. Lue (ed.), Oak Ridge Tokamak Experimental Power Reactor Study Reference Design, 1976 – Part 3, Magnetics, ORNL/TM-5574, Oak Ridge, TN (to be published).
7. J.E.C. Williams, Superconductivity and Its Applications, Pion Ltd., London, 1970.
8. H. Brechna, Superconducting Magnet Systems, Springer-Verlag, New York, 1973.
9. W. J. Carr, J. Appl. Phys. 45:929 (1974).
10. J. E. Akin and W. H. Gray, "Finite Element Stress Analysis of High Field Solenoids," Proc. 6th Symposium on Engineering Problems of Fusion Research (1976).
11. J. E. Akin and W.C.T. Stoddart, Computer Programs for Implementing the Finite Element Method, Report ESM 75-1, Department of Engineering Science and Mechanics, University of Tennessee, Knoxville, TN (August 1975).

ORNL DWG. 75-17034

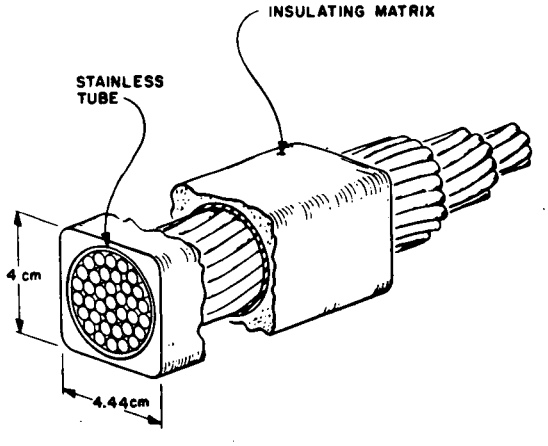

Fig. 1. Round bundle with 37 strands enclosed in rectangular conduit showing transposition of strands.

Table 1. Poloidal Field Magnet Conductor Parameters from Ref. 5

Symbol	Value	Units	Description
			NbTi
J_c	7×10^8 @ 4.2°K, 7 T	A/m^2	Critical current density
J	3.54×10^8	A/m^2	Operating current density
			Matrix
ρ_{Cu}	4×10^{-10} @ 7 T	Ω-m	Cu resistivity
ρ_{CuNi}	5×10^{-8} @ 7 T	Ω-m	CuNi resistivity
			Structure
ρ_{ss}	5×10^{-7} @ 7 T	Ω-m	Stainless steel resistivity
			Wire
I	18.26	A	Current
d_w	5.74×10^{-4}	m	Diameter
--	0.2 : 0.7 : 0.1	--	Composition NbTi : Cu : CuNi
d_f	4	μm	Filament diameter
n_f	4106	--	Number of filaments
--	5.15×10^{-3}	m	Twist pitch
			Strand
d_s	3.9×10^{-3}	m	Diameter
n_w	37	--	Number of wires
			Other
n_s	37	--	Number of strands
--	3.48×10^{-2}	m	Bundle outside diameter
--	1:1	--	Metal/helium area
--	5×10^{-4}	m	SS tube wall thickness
--	3.5×10^{-2}	m	SS tube wall diameter

Table 2. Comparison of the Superconductor Losses in Two Segments of the Central Solenoid; Each 1/8 of the Total Coil Length is Located at the End of the Solenoid and the Other Near the Midplane

	Hysteresis		Coupling		Eddy Current (SS)		Stress-Induced	
	Middle Segment (J)	End Segment (J)	Middle Segment (J)	End Segment (J)	Middle Segment (J)	End Segment (J)	Middle Segment (J)	End Segment (J)
Central solenoid only	1400	1600	109	98	751	674	2750	1590
Outboard magnets only	210	230	3.2	9.6	22	66	50	1230
Combined	1610	1830	112.2	107.6	773	740	2800	2820

ORNL DWG 76-18428

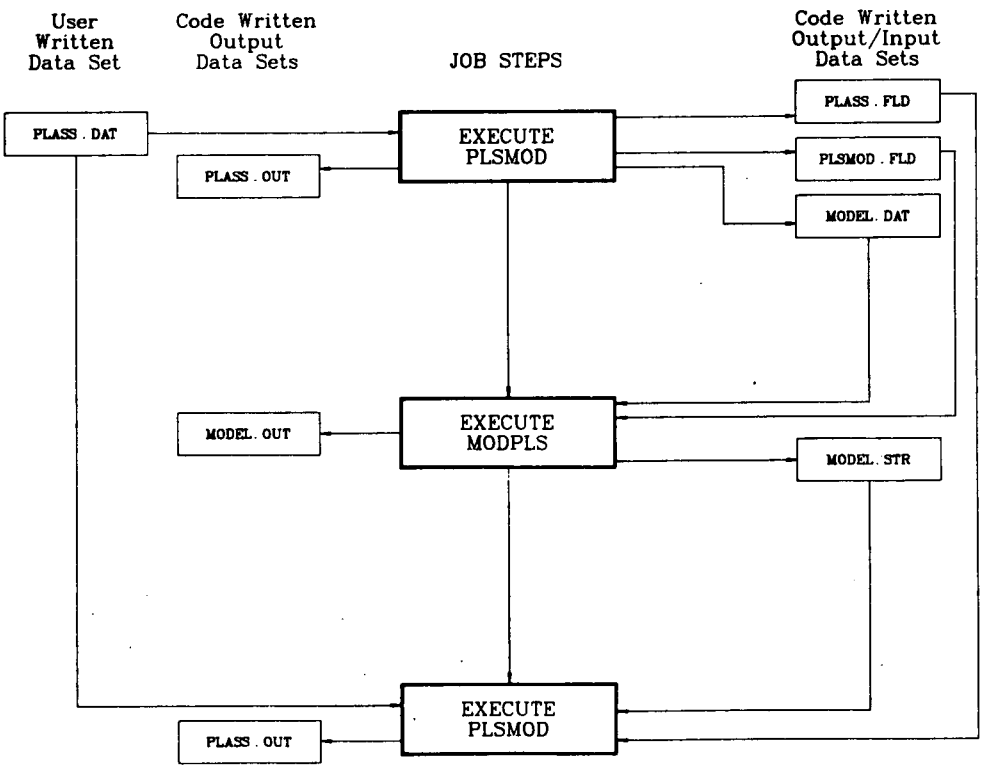

Fig. 2. Flow chart showing the relationships between job steps and data sets.

ORNL DWG 76-18429

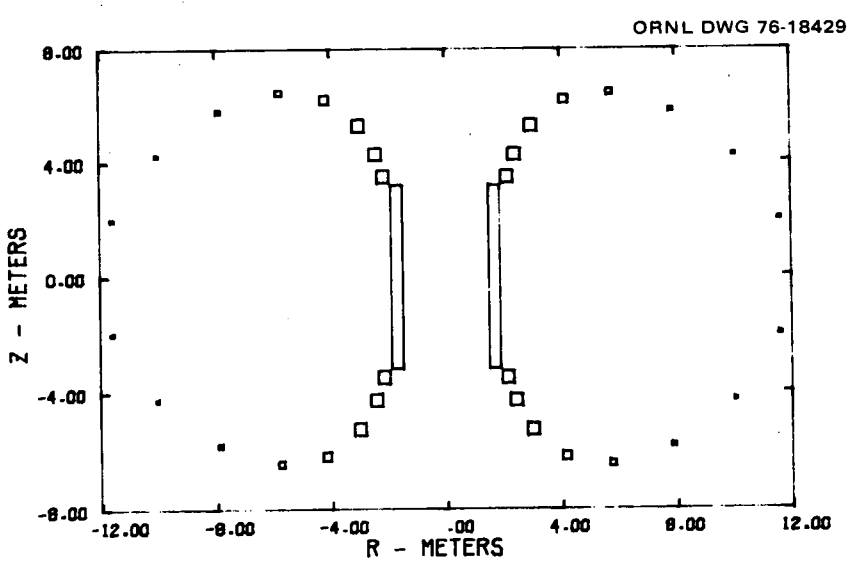

Fig. 3. Poloidal Coil Geometry

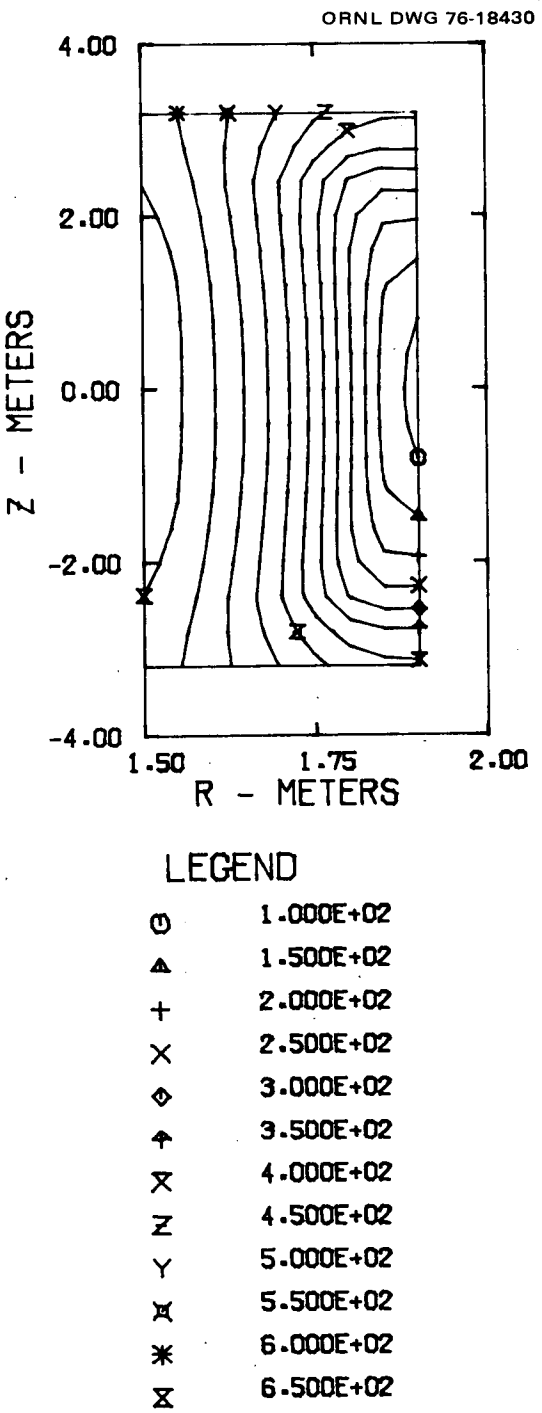

Fig. 4. Contours of constant hysteresis loss in J/M**3 versus position in the central solenoid of the ORNL EPR reference design. The losses are due to self-field.

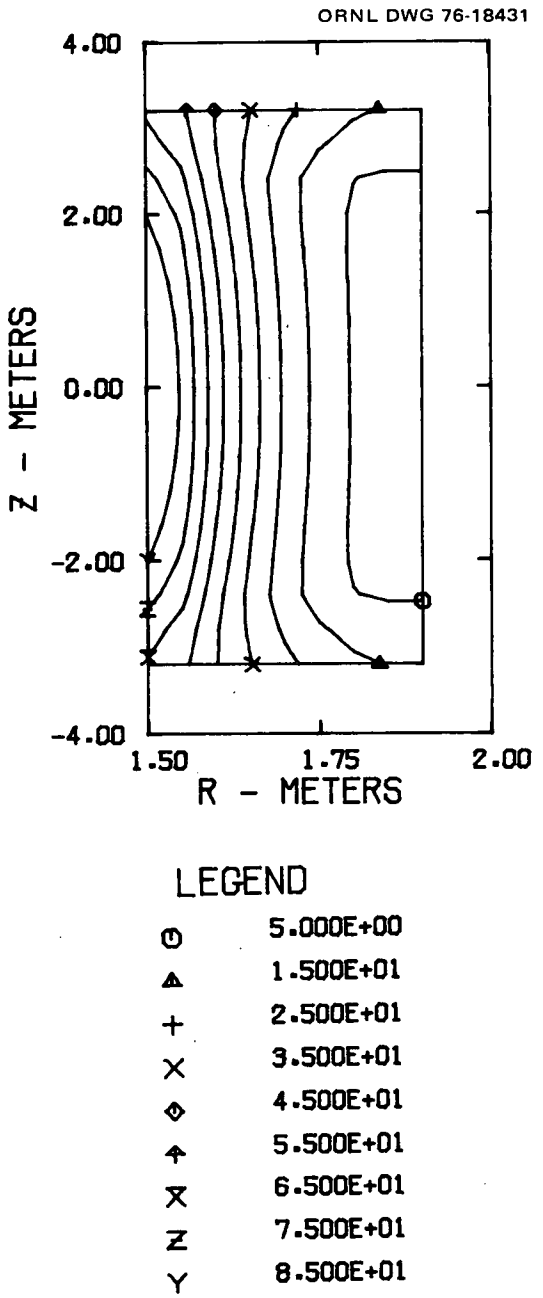

Fig. 5. Contours of constant coupling loss in J/M**3 versus position in the central solenoid of the ORNL EPR reference design. The losses are due to self-field.

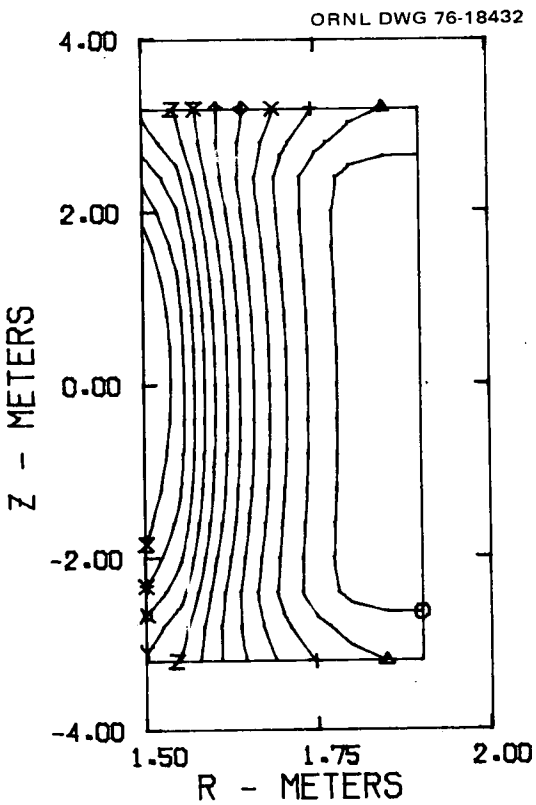

LEGEND

⊙	5.000E+01
▲	1.000E+02
+	1.500E+02
×	2.000E+02
◇	2.500E+02
✦	3.000E+02
⧖	3.500E+02
Z	4.000E+02
Y	4.500E+02
⌘	5.000E+02
✳	5.500E+02
⧖	6.000E+02

Fig. 6. Contours of constant eddy current loss in J/M**3 versus position in the central solenoid of the ORNL EPR reference design. The losses are due to self-field.

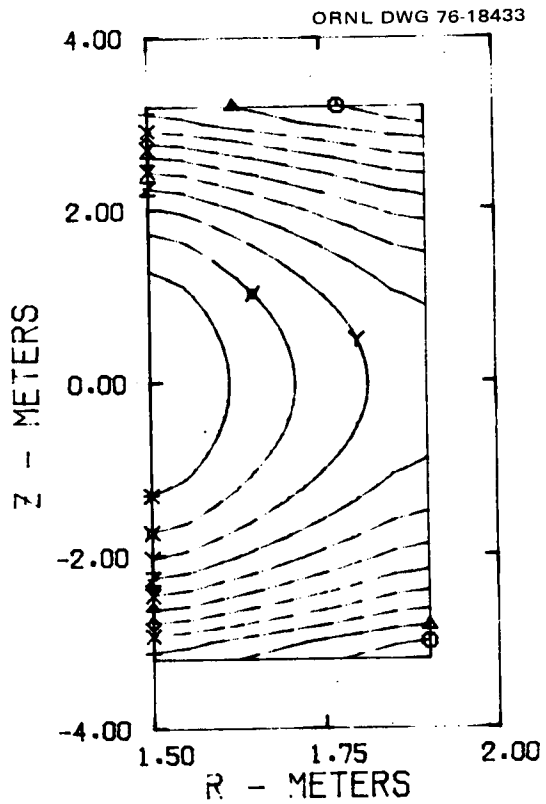

LEGEND

⊙	3.500E+02
▲	4.000E+02
+	4.500E+02
×	5.000E+02
◇	5.500E+02
✦	6.000E+02
⧖	6.500E+02
Z	7.000E+02
Y	7.500E+02
⌘	8.000E+02
✳	8.500E+02

Fig. 7. Contours of constant stress-induced heat production in J/M**3 versus position in the central solenoid of the ORNL EPR reference design. The losses are due to self-field.

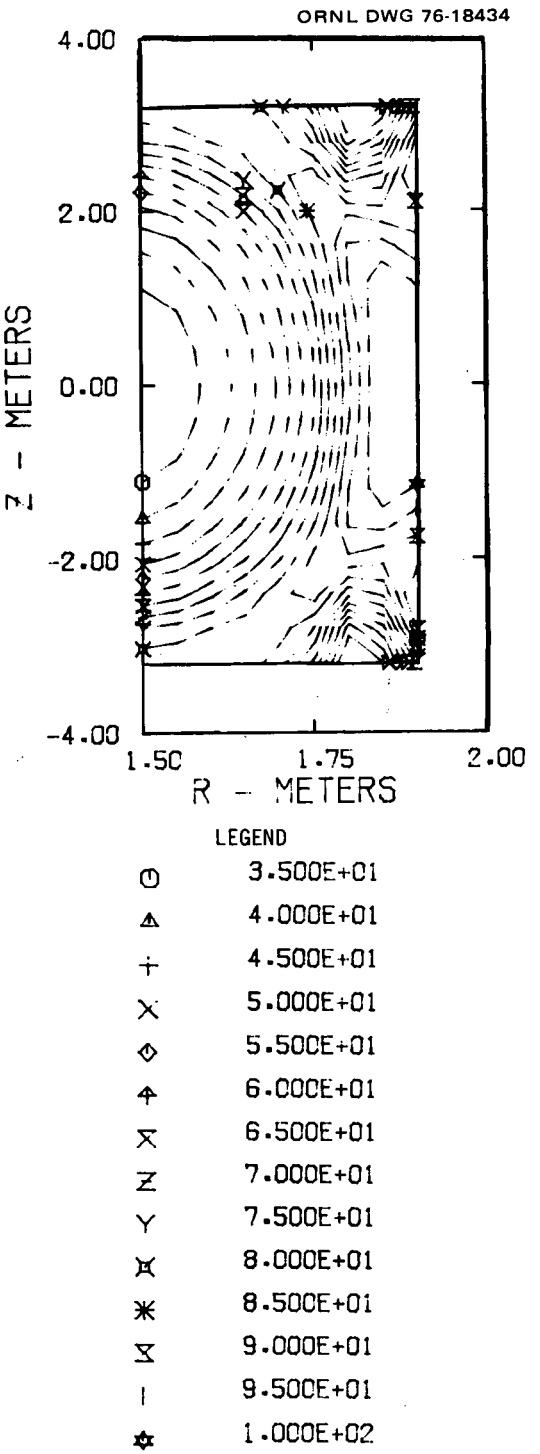

Fig. 8. Contours of constant hysteresis loss in J/M**3 versus position in the central solenoid of the ORNL EPR reference design. The losses are due to other poloidal magnets.

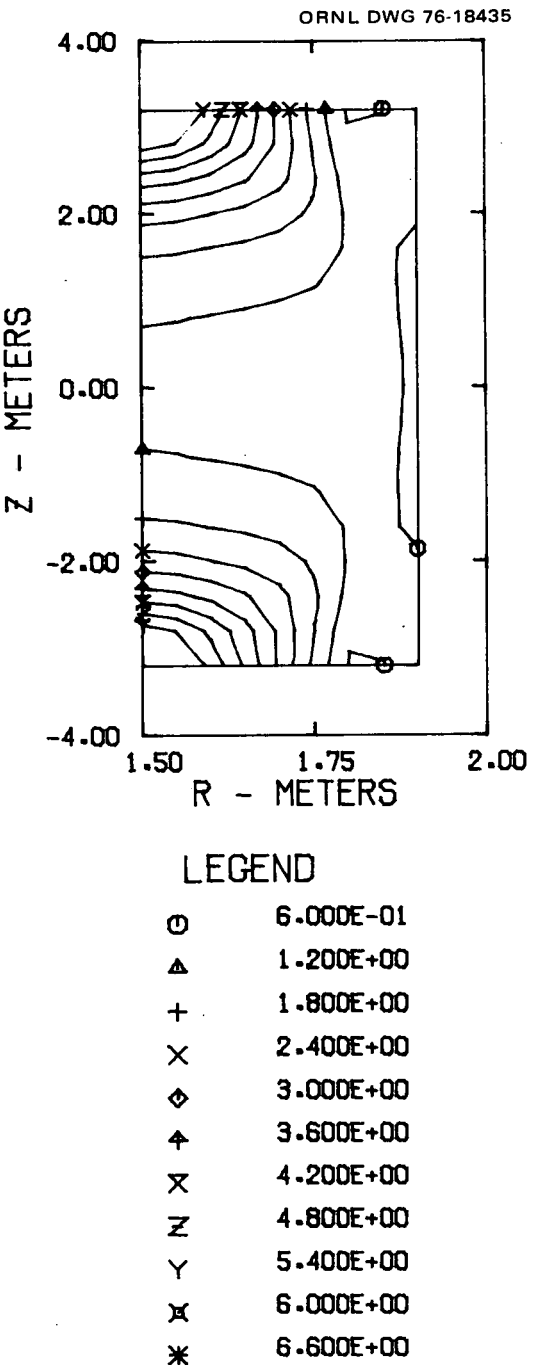

Fig. 9. Contours of constant coupling loss in J/M**3 versus position in the central solenoid of the ORNL EPR reference design. The losses are due to other poloidal magnets.

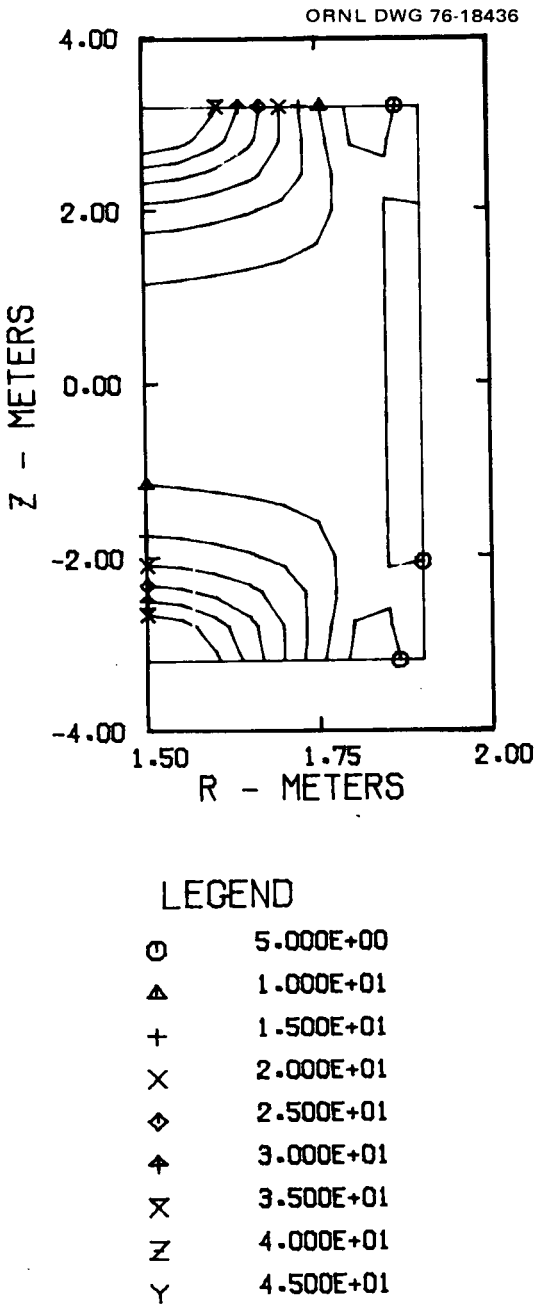

Fig. 10. Contours of constant eddy current loss in J/M**3 versus position in the central solenoid of the ORNL EPR reference design. The losses are due to other poloidal magnets.

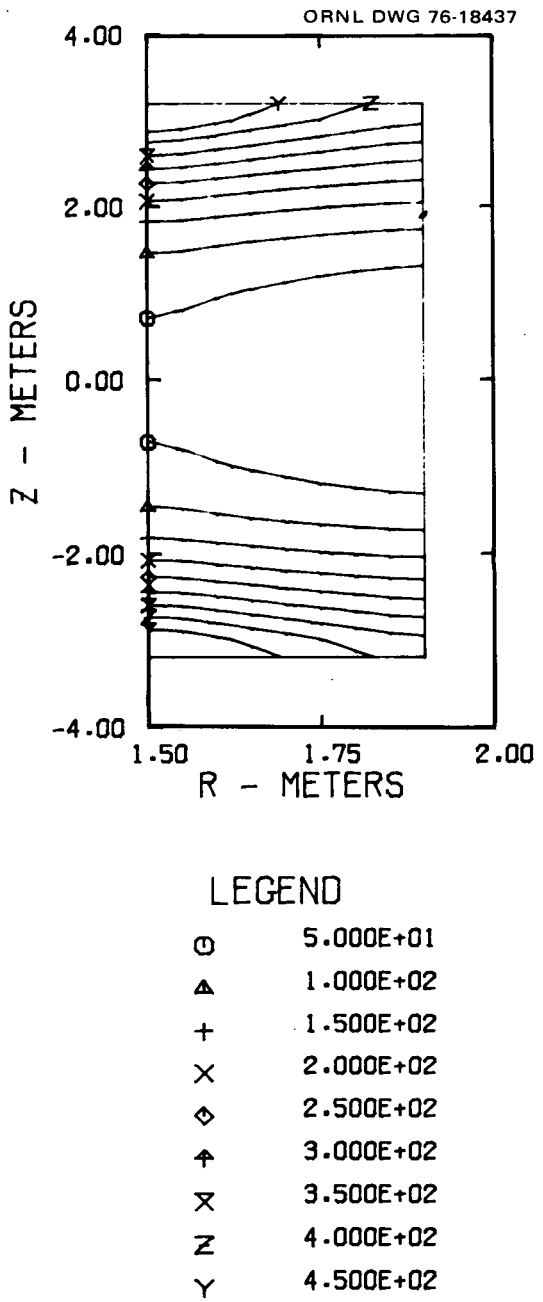

Fig. 11. Contours of constant stress-induced heat production in J/M**3 versus position in the central solenoid of the ORNL EPR reference design. The losses are due to other poloidal magnets.

INTERNAL DISTRIBUTION

1. W. C. Anderson
2. J. K. Ballou
3. R. L. Brown
4. E. H. Bryant
5. P. B. Burn
6. W. D. Cain
7. D. D. Cannon
8. J. F. Clarke
9. F. L. Culler
10. L. Dresner
11. J. F. Ellis
12. W. A. Fietz
13. W. H. Gray
14. P. N. Haubenreich
15. J. P. Kois
16. G. G. Kelley
17. C. G. Lawson
18. C. J. Long
19. H. M. Long
20. J. K. Lovin
21-25. M. S. Lubell (5)
26. J. W. Lue
27. J. N. Luton
28. H. C. McCurdy
29. J. R. Miller
30. R. V. Miskell
31. O. B. Morgan
32. H. Pih
33. H. Postma
34. M. Roberts
35. M. W. Rosenthal
36. R. E. Schwall
37. T. E. Shannon
38. S. S. Shen
39. J. E. Simpkins
40. D. Steiner
41. W. C. T. Stoddart
42. P. B. Thompson
43. P. L. Walstrom
44. H. T. Yeh
45. A. Zucker
46-47. C. R. Library (2)
48. CTR Reports Office
49. Document Ref. Section
50-51. Lab Records Dept. (2)
52. Lab Records, ORNL, R.C.
53. Patent Office
54-55. T. D. Library (2)

EXTERNAL DISTRIBUTION

56. E. Adam, Airco, 100 Mountain Avenue, Murray Hill, NJ 07974.
57. J. W. Beal, DMFE, ERDA, Mail Stop G-234, Washington, DC 20545.
58. R. W. Boom, 513 Engineering Research Building, University of Wisconsin, Madison, WI 53706.
59. D. L. Coffey, American Magnetics Inc., P. O. Box R, Oak Ridge, TN 37830.
60. D. N. Cornish, Lawrence Livermore Laboratory, P. O. Box 808, Livermore, CA 94550.
61. M. D'Agostino, Grumman Aerospace Corp., Bethpage, NY 11714.
62. J. E. Darby, Jr., CTR Program, D208, Argonne National Laboratory, 9700 South Cass Avenue, Argonne, IL 60439.
63. R. W. Derby, Magnetics Engineering Associates, 247 Third Street, Cambridge, MA 02141.
64. Director, Research & Technical Services Division, ERDA, Oak Ridge Operations, Oak Ridge, TN 37830.
65. R. W. Fast, Manager, Experimental Facilities, National Accelerator Laboratory, P. O. Box 500, Batavia, IL 60510.
66. J. J. Ferrante, General Electric Co., Schenectady, NY 12345.
67. J. File, Princeton University, Plasma Physics Laboratory, Princeton, NJ 08540.
68. W. S. Gilbert, Lawrence Berkeley Laboratory, University of California, Berkeley, CA 94120.

69. R. W. Gould, Dept. of Applied Physics, California Institute of Technology, Pasadena, CA 91109.
70. H. Grad, Courant Institute, New York University, 251 Mercer Street, New York, NY 10012.
71. E. Gregory, Airco, 100 Mountain Avenue, Murray Hill, NJ 07974.
72. W. V. Hassenzahl, Los Alamos Scientific Laboratory, P. O. Box 1663 Los Alamos, NM 87544.
73. C. D. Henning, DMFE, ERDA, Mail Stop G-234, Washington, DC 20545.
74. G. K. Hess, DMFE, ERDA, Mail Stop G-234, Washington, DC 20545.
75. C. K. Jones, Manager, Cryogenic Research Laboratory, Westinghouse Electric Corporation, R & D Center, Pittsburgh, PA 15235.
76. E. E. Kintner, DMFE, ERDA, Mail Stop G-234, Washington, DC 20545.
77. H. L. Laquer, Los Alamos Scientific Laboratory, P. O. Box 1663, Los Alamos, NM 87544.
78. C. Laverick, 543 Hampshire Lane, Boling Brook, IL 60439.
79. J. A. Mayhall, Lockheed, P. O. Box 1103, Huntsville, AL 35807.
80. D. B. Montgomery, MIT, National Magnet Laboratory, 170 Albany Street, Cambridge, MA 02139.
81. F. Moon, Dept. of Theoretical & Applied Mechanics, Cornell University, Ithaca, NY 14850.
82. R. W. Moses, Jr., University of Wisconsin, Madison, WI 53706.
83. J. R. Powell, Brookhaven National Laboratory, Upton, NY 11973.
84. J. R. Purcell, General Atomic Company, P. O. Box 81608, San Diego, CA 92138.
85. P. Reardon, PPPL, Princeton Univ., P. O. Box 451, Princeton, NJ 08540.
86. J. D. Rogers, Q-26, Los Alamos Scientific Laboratory, P. O. Box 1663, Los Alamos, NM 87544.
87. D. J. Rose, Dept. of Nuclear Engineering, Massachusetts Institute of Technology, Cambridge, MA 02139.
88. C. H. Rosner, Intermagnetics General Corp., Charles Industrial Park, New Karner Road, Guilderland, NY 12084.
89. W. B. Sampson, Brookhaven National Laboratory, Upton, Long Island, NY 11973.
90. Z. J. J. Stekly, Magnetic Corporation of American, 179 Bear Hill Road, Waltham, MA 02154.
91. B. P. Strauss, Fermi National Accelerator Laboratory, P. O. Box 500, Batavia, IL 60510.

92-118. TIC, Oak Ridge, TN 37830. (27)

119. C. E. Taylor, Lawrence Livermore Laboratory, P. O. Box 808, L-384 Livermore, CA 94551.
120. R. Thomas, General Atomic Company, P. O. Box 81608, San Diego, CA 92138.
121. C. von Keszycki, Grumman Aerospace Corp., Research Center, Building 26, Bethpage, NY 11714.
122. S. T. Wang, Argonne National Laboratory, 9700 South Cass Avenue, Argonne, IL 60439.
123. J. M. Williams, DMFE, ERDA, Mail Stop G-234, Washington, DC 20545.
124. S. L. Wipf, Q-26, Los Alamos Scientific Research Laboratory, P. O. Box 1663, Los Alamos, NM 87544.
125. J. Wong, Supercon, Inc., 9 Erie Drive, Natick, MA 01760.
126. H. H. Woodson, Chairman, Dept. of Electrical Engineering, University of Texas at Austin, Austin, TX 78712.
127. E. J. Ziurys, DMFE, ERDA, Mail Stop G-234, Washington, DC 20545.